

METASTABLE INTERNAL LAYER DYNAMICS FOR THE VISCOUS CAHN-HILLIARD EQUATION

Luis G. Reyna and Michael J. Ward

Dedicated to Chuck Lange

ABSTRACT. A formal asymptotic method is used to derive a differential-algebraic system of equations characterizing the metastable motion of a pattern of n ($n \geq 2$) internal layers for the one-dimensional viscous Cahn-Hilliard modeling slow phase separation. Similar slow motion results are obtained for the Cahn-Hilliard equation and the constrained Allen-Cahn equation by introducing a homotopy parameter into the viscous Cahn-Hilliard equation and letting this parameter take on limiting values. For each of these phase separation models, the asymptotic results for the slow internal layer motion associated with two-layer metastable patterns are found to compare very favorably over very long time intervals with corresponding full numerical results computed using a finite-difference scheme. Finally, an example is given that clearly illustrates the very sensitive effect of boundary conditions on metastable internal layer dynamics.

1. Introduction

We study the metastable internal layer motion, in one spatial dimension, associated with the viscous Cahn-Hilliard equation modeling the phase separation of a binary mixture. In dimensionless variables, this phase separation model, introduced in [19], is given by

$$u_t = -(\epsilon^2 u_{xx} + Q(u) - \kappa u_t)_{xx}, \quad -1 < x < 1, \quad t > 0, \quad (1.1)$$

with appropriate boundary and initial conditions. Here, u is the concentration of one of the two species, $\epsilon \ll 1$ is an interfacial energy parameter, and $Q(u) = -V'(u)$ is a non-monotone function defined in terms of a double-well potential $V(u)$. The precise assumptions on the form of $Q(u)$ are given in (2.2). The boundary conditions for (1.1) are such that the mass $m = \int_{-1}^1 u(x, t) dx$ is conserved. In (1.1), the term κu_{txx} accounts for viscous relaxation effects in the binary mixture and $\kappa \geq 0$ is the viscosity coefficient. The well-known Cahn-Hilliard equation (cf. [4]) is obtained by setting $\kappa = 0$. Since $Q(u)$ is non-monotone, the reduced equation $u_t = -[Q(u)]_{xx}$ is an ill-posed backward heat equation for some range of u . The terms $-\epsilon^2 u_{xxxx}$ and κu_{txx} represent a gradient energy regularization and a viscous regularization, respectively, of this ill-posed reduced equation. Results concerning the equilibrium solutions and the long time behavior of solutions associated with this viscous regularization are given

Received August 3, 1994, revised January 20, 1995.

1991 *Mathematics Subject Classification*: 35B25, 80A22, 65N06.

Key words and phrases: dynamic metastability, Cahn-Hilliard, finite-difference, differential-algebraic system.

This work was supported by NSERC grant 5-81541.

in [20]. A more detailed discussion concerning the physical motivation for (1.1) is given in [19] and [20] (see also the references therein).

For $\epsilon \rightarrow 0$, the qualitative features of the dynamics associated with (1.1) are as follows. Through a very intricate transient process, a pattern of internal layers is formed from initial data over an $O(1)$ time interval. However, once this pattern has formed, the subsequent motion of the internal layers is exponentially slow. For the Cahn-Hilliard equation, the occurrence of this metastable motion for a two-layer pattern has been proved in [1] from a dynamical systems viewpoint and in [3] using energy methods combined with some results of [11]. In [11], similar slow motion results were obtained for a system of Cahn-Hilliard-type equations. We are not aware of any analogous slow motion results for the viscous Cahn-Hilliard equation.

To complement these previous results which establish the existence of the slow motion for the Cahn-Hilliard equation, we give an *explicit* characterization of metastable internal layer motion for the more general viscous Cahn-Hilliard equation (1.1). Specifically, for $\epsilon \rightarrow 0$, we use formal asymptotic methods to derive a differential-algebraic system of equations for the locations of the internal layers associated with an n -layer metastable pattern. In the derivation, we assume that the internal layers are widely separated, and thus, we do not account for internal layer collisions. To obtain similar slow motion results for two related phase separation models, it is convenient in the analysis to modify (1.1) by introducing a homotopy parameter. By letting this parameter take on certain limiting values, we obtain explicit asymptotic results for the metastable motion associated with the Cahn-Hilliard equation and the constrained Allen-Cahn equation.

Metastable internal layer motion has been studied recently for other evolution equations. The internal layer dynamics for the Allen-Cahn equation and some related equations has been studied from a dynamical systems viewpoint in [5], [9], and [15] and by formal asymptotic methods in [18], [21], and [25]. Similar slow motion behavior has been shown in [14], [16], and [22] to occur for a class of viscous shock problems. The method we use to explicitly characterize the internal layer dynamics for (1.1) in the absence of any layer collisions is an extension of the projection method used successfully in [21], [22], and [25] to treat these related problems. This method combines the method of matched asymptotic expansions with certain spectral properties associated with the underlying linearized operator. For the Allen-Cahn equation and the viscous shock problem, analytical results obtained from the projection method have been favorably compared in [21] and [22] with full numerical results and, in a few cases, with explicit analytical solutions to the full perturbed problems.

For a two-layer metastable pattern, we compare our asymptotic metastability results for (1.1) with corresponding full numerical results computed using a finite-difference scheme. The asymptotic and numerical results are shown to be in very close agreement over very long time intervals. Moreover, the numerical method is able to accurately track the motion of the internal layers on a time interval of order 10^{11} . This time interval is significantly longer than the computational time interval reported in the previous numerical studies of slow motion behavior for the Cahn-Hilliard equation given in [8] and by McKinney (described in [1]).

In a sequel to this paper, we plan to examine both asymptotically and numerically the coarsening process associated with (1.1). This process describes the mechanism by which an initial metastable pattern of n internal layers cascades, by way of layer collapse events, to metastable patterns with fewer and fewer layers. The dynamic

metastability results herein for patterns with widely separated layers provide the first step in characterizing the coarsening process in the presence of a mass constraint. In [25], a hybrid asymptotic-numerical method was used to study the coarsening process for the simpler Allen-Cahn equation in the absence of a mass constraint.

We also investigate the sensitive effect of boundary conditions on metastable dynamics. For a specific form of the Allen-Cahn equation defined on the infinite line, we show that the inclusion of artificial boundary conditions used to truncate the infinite domain to a finite domain leads to spurious metastable internal layer dynamics (see [24] for some related work). In a more general context, we believe that the analysis of this example has implications for the accurate numerical computation of other types of weakly interacting localized structures on the infinite line.

The outline of the paper is as follows. In §2, we derive asymptotic equations of motion for the locations of the internal layers corresponding to a two-layer metastable pattern for (1.1). Similar asymptotic results are obtained for the Cahn-Hilliard equation and the constrained Allen-Cahn equation. In §3, these asymptotic results for the metastable motion are compared with corresponding full numerical results. In §4, the asymptotic results of §2 are extended to treat a metastable pattern of n ($n \geq 2$) internal layers. Finally, in §5, we give an example illustrating the sensitive effect of artificial boundary conditions on metastable internal layer dynamics.

2. A two-layer metastable pattern for the viscous Cahn-Hilliard equation

We consider the viscous Cahn-Hilliard equation in the form

$$(1 - \alpha)u_t = -(\epsilon^2 u_{xx} + Q(u) - \alpha \kappa u_t)_{xx}, \quad -1 < x < 1, \quad t > 0, \quad (2.1a)$$

$$u(x, 0) = u_0(x), \quad u_x(\pm 1, t) = u_{xxx}(\pm 1, t) = 0. \quad (2.1b)$$

Here $\kappa > 0$ and $Q(u)$ is the derivative of a double-well potential $V(u)$. We assume that $Q(u)$ has exactly three zeroes on the interval $[s_-, s_+]$, located at $u = s_- < 0$, $u = 0$, and $u = s_+ > 0$, with

$$Q'(s_{\pm}) < 0, \quad Q'(0) > 0, \quad V(s_+) = 0, \quad V(u) = -\int_{s_-}^u Q(\eta) d\eta. \quad (2.2)$$

Since (2.1a) is unchanged upon adding a constant to $Q(u)$, we can choose $V(s_+) = 0$ without loss of generality.

In (2.1a), α is a homotopy parameter satisfying $0 \leq \alpha \leq 1$. When $0 \leq \alpha < 1$, the mass $m = \int_{-1}^1 u(x, t) dx$ is conserved for (2.1). For $\alpha = 0$, (2.1) reduces to the Cahn-Hilliard equation. For $\alpha = 1$ and $\kappa = 1$, we impose the mass constraint on (2.1) to obtain the constrained Allen-Cahn equation,

$$u_t = \epsilon^2 u_{xx} + Q(u) - \sigma_c(t), \quad u_x(\pm 1, t) = 0, \quad \int_{-1}^1 u(x, t) dx = m. \quad (2.3)$$

In (2.3), $\sigma_c(t)$ is determined by the mass constraint. Some results for the constrained Allen-Cahn equation in two spatial dimensions are given in [23]. The unconstrained Allen-Cahn equation is obtained by setting $\sigma_c(t) = 0$ in (2.3) and disregarding the mass constraint. In the derivation of metastable dynamics below, we assume that the initial condition for (2.1) is such that m satisfies $2s_- < m < 2s_+$.

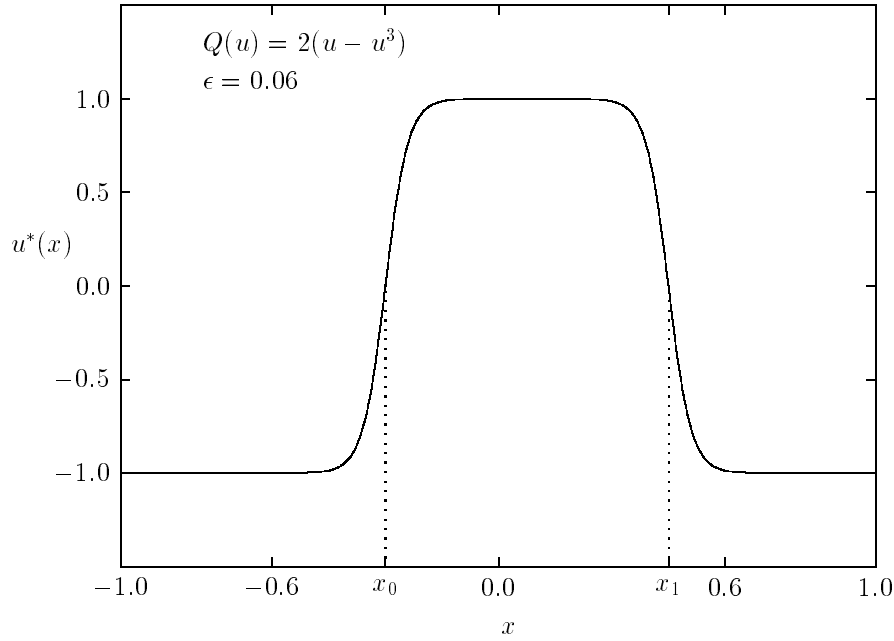


FIGURE 1. Plot of $u^*(x)$ given by (2.5) with $u_s(z) = \tanh(z)$ and $s_+ = 1$, that approximates a two-layer metastable pattern for (2.1).

To analyze metastable behavior for (2.1), it is convenient to rewrite (2.1) in the form

$$\alpha \kappa u_t = \epsilon^2 u_{xx} + Q(u) - \sigma, \quad u_x(\pm 1, t) = 0, \quad (2.4a)$$

$$(1 - \alpha)u_t = -\sigma_{xx}, \quad \sigma_x(\pm 1, t) = 0, \quad (2.4b)$$

with $u(x, 0) = u_0(x)$. The transient process associated with the formation of a metastable pattern from initial data $u_0(x)$ is very complicated and will not be discussed. Instead, we assume that $u_0(x)$ is such that a two-layer metastable pattern for (2.1), with a structure as shown in Figure 1, is formed on an $O(1)$ time interval. For $\epsilon \rightarrow 0$, it was shown in [2, 6, 21] that σ is exponentially small when this two-layer pattern is in equilibrium. In our derivation below of metastable internal layer dynamics, we assume that σ also is exponentially small during the metastable evolution.

The two-layer metastable pattern for (2.1) shown in Figure 1 is represented by the approximate form $u(x, t) \sim u^*(x)$, where

$$u^*(x) = u^*(x; x_0, x_1) \equiv u_s[\epsilon^{-1}(x - x_0)] + u_s[\epsilon^{-1}(x_1 - x)] - s_+. \quad (2.5)$$

Here $x_0 = x_0(t)$, $x_1 = x_1(t)$, $x_0 < x_1$, and $u_s(z)$ is the unique heteroclinic orbit connecting s_- and s_+ , which satisfies

$$u_s''(z) + Q[u_s(z)] = 0, \quad -\infty < z < \infty; \quad u_s(0) = 0; \quad u_s'(z) > 0; \quad (2.6a)$$

$$u_s(z) \sim s_+ - a_+ e^{-\nu_+ z}, \quad z \rightarrow \infty; \quad u_s(z) \sim s_- + a_- e^{\nu_- z}, \quad z \rightarrow -\infty. \quad (2.6b)$$

The positive constants ν_{\pm} and a_{\pm} in (2.6b) are defined by

$$\begin{aligned} \nu_{\pm} &= (-Q'(s_{\pm}))^{1/2}, \\ \log a_{\pm} &= \log(\pm s_{\pm}) + \int_0^{s_{\pm}} \left(\frac{\pm \nu_{\pm}}{[2V(\eta)]^{1/2}} + \frac{1}{\eta - s_{\pm}} \right) d\eta. \end{aligned} \quad (2.7)$$

Since $u_s(0) = 0$, the curves $x = x_0(t)$ and $x = x_1(t)$ closely determine the locations of the zeroes of $u(x, t)$ during the slow evolution.

To derive equations of motion for $x_0(t)$ and $x_1(t)$, we use a projection method, which is an extension of a similar method used in [21, 22, 25] to treat other problems exhibiting dynamic metastability phenomena. This method is based on an asymptotic analysis of the quasi-steady linearization of (2.4) about $u = u^*$ and $\sigma = 0$. To obtain the form of this quasi-steady linearization, we substitute $u(x, t) = u^*(x; x_0, x_1) + w(x, t)$ into (2.4), where w satisfies $w \ll u^*$ and $w_t \ll u_t^*$. Assuming that $\sigma = O(u_t^*) \ll 1$, we then obtain the following quasi-steady approximate system from (2.4) and (2.6b):

$$\epsilon^2 w_{xx} + Q'(u^*)w = \sigma + E(x) + \alpha \kappa u_t^*, \quad (2.8a)$$

$$w_x(-1, t) = -u_x^*(-1) \sim -\epsilon^{-1} a_- \nu_- e^{-\epsilon^{-1} \nu_- (1+x_0)}, \quad (2.8b)$$

$$w_x(1, t) = -u_x^*(1) \sim \epsilon^{-1} a_- \nu_- e^{-\epsilon^{-1} \nu_- (1-x_1)}, \quad (2.8c)$$

$$\sigma_{xx} = (1 - \alpha) \epsilon^{-1} \sum_{j=0}^1 (-1)^j \dot{x}_j u_s' [\epsilon^{-1} (-1)^j (x - x_j)], \quad \sigma_x(\pm 1, t) = 0. \quad (2.8d)$$

Here $\dot{x}_j \equiv dx_j/dt$ and $E(x) = E(x; x_0, x_1)$ is defined by

$$E(x; x_0, x_1) = \sum_{j=0}^1 Q(u_s[\epsilon^{-1} (-1)^j (x - x_j)]) - Q(u^*). \quad (2.9)$$

The term $E(x)$ represents the exponentially weak interactions between the internal layers.

Next, we integrate (2.8d) to derive

$$\begin{aligned} \sigma_x(x, t) &= (1 - \alpha) \dot{x}_0 (u_s[\epsilon^{-1} (x - x_0)] - s_-) \\ &\quad + (1 - \alpha) \dot{x}_1 (u_s[\epsilon^{-1} (x_1 - x)] - s_+). \end{aligned} \quad (2.10)$$

From (2.6b) and (2.10), it is clear that $\sigma_x(-1, t)$ is exponentially small. Moreover, since $\dot{x}_1 - \dot{x}_0 = 0$, which is an obvious consequence of the mass constraint, it also follows from (2.6b) that $\sigma_x(1, t)$ is exponentially small. We claim that these exponentially small errors in satisfying the boundary conditions for σ can be neglected in the derivation of the asymptotic equations of motion for $x_j(t)$. (The justification for this claim is described below following (2.18b).) Then integrating (2.10), we obtain

$$\sigma(x, t) = (1 - \alpha) \dot{x}_0 M_0(x; x_0) + (1 - \alpha) \dot{x}_1 M_1(x; x_1) + \sigma_c(t). \quad (2.11)$$

Here $\sigma_c(t)$ is an unknown function to be determined, and M_0 and M_1 are defined by

$$\begin{aligned} M_0(x; x_0) &= \int_{-1}^x (u_s[\epsilon^{-1} (\eta - x_0)] - s_-) d\eta, \\ M_1(x; x_1) &= \int_{-1}^x (u_s[\epsilon^{-1} (x_1 - \eta)] - s_+) d\eta. \end{aligned} \quad (2.12)$$

The problem for w then is obtained by substituting (2.5) and (2.11) in (2.8a).

Now consider the eigenvalue problem associated with (2.8a,b,c):

$$\epsilon^2 \phi_{xx} + Q'(u^*) \phi = \lambda \phi, \quad -1 < x < 1, \quad (\phi, \phi) = 1, \quad (2.13a)$$

$$\phi_x(-1) = 0, \quad \phi_x(1) = 0. \quad (2.13b)$$

The inner product in (2.13a) is defined by $(g, h) \equiv \int_{-1}^1 gh \, dx$. For $\epsilon \rightarrow 0$, the first two eigenvalues of (2.13) are exponentially small while the remaining eigenvalues are bounded away from zero (cf. [5]). The eigenfunctions $\phi_j(x)$ for $j = 0, 1$ which correspond to these exponentially small eigenvalues are given asymptotically for $\epsilon \rightarrow 0$ by $\phi_j(x) \sim R_j u'_s [(-1)^j \epsilon^{-1}(x - x_j)]$, where R_j is a normalization constant.

Next, we expand the solution to (2.8a,b) in terms of the eigenfunctions of (2.13) as

$$w = \sum_{j=0}^{\infty} \frac{A_j}{\lambda_j} \phi_j. \quad (2.14a)$$

Upon integrating by parts and using Green's identity, we derive

$$A_j = (E, \phi_j) + (\sigma, \phi_j) + \alpha \kappa(u_t^*, \phi_j) - B_j, \quad (2.14b)$$

$$B_j = \epsilon^2 [\phi_j(1)w_x(1, t) - \phi_j(-1)w_x(-1, t)].$$

Since $\lambda_j \rightarrow 0$ as $\epsilon \rightarrow 0$ for $j = 0, 1$, a necessary condition for the solvability of (2.8a,b,c) in this limit is that $A_j = 0$ for $j = 0, 1$. By substituting (2.11) into these limiting solvability conditions, we obtain the following evolution equations for x_0 and x_1 :

$$(1 - \alpha)\dot{x}_0(M_0, \phi_0) + (1 - \alpha)\dot{x}_1(M_1, \phi_0) + (\sigma_c, \phi_0) + (E, \phi_0) + \alpha \kappa(u_t^*, \phi_0) \sim B_0, \quad (2.15a)$$

$$(1 - \alpha)\dot{x}_0(M_0, \phi_1) + (1 - \alpha)\dot{x}_1(M_1, \phi_1) + (\sigma_c, \phi_1) + (E, \phi_1) + \alpha \kappa(u_t^*, \phi_1) \sim B_1. \quad (2.15b)$$

The system (2.15) gives two equations for the three unknowns $x_0(t)$, $x_1(t)$, and $\sigma_c(t)$. An additional equation results from replacing u by u^* in the mass constraint $m = \int_{-1}^1 u(x, t) \, dx$. For $\epsilon \rightarrow 0$, we evaluate this approximation to the mass constraint to show that $d_1 = x_1(t) - x_0(t)$ is independent of t and is given by

$$d_1 = \frac{\tilde{m} - 2s_-}{s_+ - s_-}, \quad \tilde{m} \equiv m - 2\epsilon(\theta_- - \theta_+). \quad (2.16a)$$

Here $\theta_{\pm} > 0$ are defined by

$$\theta_- = \int_{-\infty}^0 [u_s(\eta) - s_-] \, d\eta, \quad \theta_+ = \int_0^{\infty} [s_+ - u_s(\eta)] \, d\eta. \quad (2.16b)$$

The constraint $2s_- < m < 2s_+$ is needed to ensure that d_1 satisfies the required inequality $0 < d_1 < 2$ in the limit $\epsilon \rightarrow 0$.

Since $\phi_j(x)$ is *localized* near $x = x_j$ and is exponentially small for $|x - x_j| = O(1)$, we can obtain explicit asymptotic equations of motion for $x_0(t)$ and $x_1(t)$ by asymptotically evaluating the various terms in (2.15) for $\epsilon \rightarrow 0$ using Laplace's method. The boundary term B_j and the inner products (E, ϕ_j) and (σ_c, ϕ_j) were evaluated

asymptotically in [21], with the result

$$\begin{aligned} (E, \phi_j) &\sim 2\epsilon a_+^2 \nu_+^2 R_j e^{-\epsilon^{-1} \nu_+ d_1}, \\ (\sigma_c, \phi_j) &\sim \epsilon R_j \sigma_c(s_+ - s_-), \quad j = 0, 1, \end{aligned} \quad (2.17a)$$

$$B_0 \sim 2\epsilon a_-^2 \nu_-^2 R_0 e^{-2\epsilon^{-1} \nu_- d_0}, \quad B_1 \sim 2\epsilon a_-^2 \nu_-^2 R_1 e^{-2\epsilon^{-1} \nu_- d_2}. \quad (2.17b)$$

Here, we have labeled $d_0 = x_0 + 1$, $d_1 = x_1 - x_0$, and $d_2 = 1 - x_1$. The remaining terms in (2.15) can be evaluated asymptotically to obtain

$$\begin{aligned} (M_0, \phi_1) &\sim \epsilon R_1 (s_+ - s_-)^2 d_1 + 2\epsilon^2 R_1 (s_+ - s_-)(\theta_- - \theta_+), \\ (M_1, \phi_0) &= O(e^{-\epsilon^{-1} c}), \\ (M_0, \phi_0) &\sim \epsilon^2 \mu R_0, \quad (M_1, \phi_1) \sim -\epsilon^2 \mu R_1, \\ (u_t^*, \phi_j) &\sim (-1)^{j+1} \dot{x}_j R_j \beta, \quad j = 0, 1. \end{aligned} \quad (2.18a)$$

In (2.18a), c is a positive constant proportional to the distance between x_1 and x_0 . In addition, $\beta > 0$ and $\mu > 0$ are defined by

$$\beta = \int_{-\infty}^{\infty} [u'_s(\eta)]^2 d\eta, \quad \mu = \int_{-\infty}^{\infty} [s_+ - u_s(\eta)] [u_s(\eta) - s_-] d\eta. \quad (2.18b)$$

The derivations of these formulas for (M_j, ϕ_k) are given in Appendix A. We emphasize that since ϕ_j is localized near $x = x_j$, the dominant contribution to the inner product (σ, ϕ_j) is insensitive to the insertion of any exponentially small boundary layers for σ near $x = \pm 1$ that are required to exactly satisfy the boundary conditions $\sigma_x(\pm 1, t) = 0$.

The function $\sigma_c(t)$ in (2.11) and the evolution equation for $d_0(t)$ are obtained by substituting (2.17) and (2.18a) into (2.15). This leads to one of our main results.

Proposition 1. *For $\epsilon \rightarrow 0$, the two-layer metastable pattern for (2.1) is represented by (2.5), where $x_0(t) = -1 + d_0(t)$, $x_1(t) = d_1 + d_0(t) - 1$, and d_1 is given in (2.16a). The distance $d_0(t)$ and the function $\sigma_c(t)$ satisfy*

$$\dot{d}_0 \sim \epsilon a_-^2 \nu_-^2 \zeta^{-1} (e^{-2\epsilon^{-1} \nu_- d_2} - e^{-2\epsilon^{-1} \nu_- d_0}), \quad (2.19a)$$

$$\begin{aligned} \sigma_c \frac{(s_+ - s_-)}{a_-^2 \nu_-^2} &\sim \left(1 - \frac{\gamma}{\zeta}\right) e^{-2\epsilon^{-1} \nu_- d_2} + \left(1 + \frac{\gamma}{\zeta}\right) e^{-2\epsilon^{-1} \nu_- d_0} \\ &\quad - \frac{2a_+^2 \nu_+^2}{a_-^2 \nu_-^2} e^{-\epsilon^{-1} \nu_+ d_1}. \end{aligned} \quad (2.19b)$$

Here ζ and γ are defined by

$$\begin{aligned} \zeta &= \alpha \kappa \beta - \epsilon^2 (1 - \alpha) \mu + \gamma, \\ \gamma &= \epsilon (1 - \alpha) (s_+ - s_-) \left[\epsilon (\theta_- - \theta_+) + (s_+ - s_-) \frac{d_1}{2} \right]. \end{aligned} \quad (2.20)$$

In (2.19) and (2.20), the constants a_{\pm} , ν_{\pm} are defined in (2.7), θ_{\pm} is defined in (2.16b), and β and μ are given in (2.18b). For the constrained Allen-Cahn equation (i.e., $\alpha = 1$ and $\kappa = 1$), $\zeta = \beta$ and $\gamma = 0$, and hence (2.19) reduces to the result given in [21] (see also [15] for some related work).

With the initial value $d_0(0) = d_0^0$, (2.19a) is readily integrated to obtain

$$d_0(t) = 1 - \frac{d_1}{2} + \frac{\epsilon}{2\nu_-} \log \left[\frac{1 + \tanh(\epsilon^{-1}\nu_-(d_0^0 - d_2^0)/2) e^{t/t_s}}{1 - \tanh(\epsilon^{-1}\nu_-(d_0^0 - d_2^0)/2) e^{t/t_s}} \right], \quad (2.21)$$

$$t_s \equiv \frac{\zeta e^{\epsilon^{-1}\nu_-(2-d_1)}}{4a_-^2 \nu_-^3}.$$

Here $d_2^0 \equiv d_2(0) = 2 - d_1 - d_0(0)$. The unstable equilibrium of (2.21) is $d_0 = d_2 = 1 - d_1/2$. It follows from (2.21) that for $\epsilon \ll 1$ and $d_0^0 > d_2^0$, the internal layer centered at x_1 will collapse against the wall at $x = 1$ at a time $t \sim \zeta e^{2\epsilon^{-1}\nu_- d_2^0} / (2a_-^2 \nu_-^3)$. Alternatively, if $d_0^0 < d_2^0$, the layer centered at x_0 will collapse against the wall at $x = -1$ when $t \sim \zeta e^{2\epsilon^{-1}\nu_- d_0^0} / (2a_-^2 \nu_-^3)$.

3. A two-layer evolution: comparison of asymptotic and numerical results

We now compare the asymptotic result (2.19a) for a two-layer metastable pattern with corresponding numerical results computed from (2.1) and (2.3) using a finite-difference method. We also outline the numerical method used to compute the solutions to (2.1) and (2.3). A full account will appear elsewhere.

3.1. The numerical method. The numerical method is based on a central finite difference scheme for the spatial discretization coupled with a third-order backward differentiation scheme (see Gear [10]) for the time discretization. Since this time integration method is of high order while still allowing for large time steps without the loss of stability, it is both accurate and efficient for tracking the motion of the internal layers over exponentially long time intervals. However, as a result of the sudden decrease in the time scale that occurs when an internal layer approaches the boundary of the domain, we found it necessary to implement a time stepping control strategy. The strategy, which monitors a bound on the error ratio between consecutive time steps, is used to reject large inaccurate time steps.

The spatial discretization for (2.1) was done using a centered fourth-order scheme for the highest derivative term and a sixth-order scheme for the lower-order terms. For smooth solutions, the formal truncation error of the spatial discretization is $O(\epsilon^2 h^4 + h^6)$. The proper numerical implementation of the boundary conditions for higher-order schemes is an important area of research [12]. For (2.1), we note that all of the odd spatial derivatives of the solution vanish at the end points of the interval. This symmetry property for the continuous problem then can be exploited to yield higher-order accurate numerical boundary conditions.

At each time step, the implementation of Newton's method requires the numerical inversion of a Jacobian. The Jacobian for the nonlinear discrete problem was evaluated analytically and inverted numerically using the subroutines for banded matrices from Linpack [17]. The explicit mass constraint for the non-local Allen-Cahn equation (2.3) results in an extra row and column in the Jacobian matrix. To numerically invert this augmented Jacobian, we used the bordering algorithm frequently employed in numerical continuation approaches for bifurcation problems [13].

The exponentially slow internal layer motion can be calculated accurately only by resolving the exponentially weak interactions between the internal layers (cf. [21]).

To ensure that these interactions are properly resolved, we adopted the conservative approach of using quadruple precision arithmetic in all of the numerical computations.

As a partial check on the computational results, the total mass was evaluated numerically at each time step by integrating the discrete solution using the mid-point rule. Since all of the odd spatial derivatives of u vanish at the end points, the Euler-Maclaurin summation formula shows that this midpoint rule is formally of infinite-order accuracy (see [7] p. 73). Our computations using 1000 meshpoints showed that the mass was conserved to many significant digits.

3.2. The comparisons. The asymptotic and numerical results for $d_0(t)$ are compared for two choices of $Q(u)$, for various values of ϵ , and for various initial conditions. The first choice of Q is the odd nonlinearity $Q(u) = Q_o(u) \equiv 2(u - u^3)$ for which $a_+ = a_-$, $\nu_+ = \nu_-$, and $\theta_+ = \theta_-$. For this form of Q , the heteroclinic orbit constants needed in (2.19)–(2.21) can be obtained analytically as

$$a_- = 2, \quad \nu_- = 2, \quad \beta = 4/3, \quad \theta_- = \log 2, \quad \mu = 2. \quad (3.1)$$

The second choice of Q is the asymmetric form $Q(u) = Q_a(u)$, where

$$Q_a(u) \equiv u(u+1)(r_0-u)(r_1-u), \quad (3.2)$$

$$r_1 = r_0 + \frac{(3+r_0-2r_0^2)}{5(r_0-1)}, \quad 1 < r_0 < 3/2.$$

Let $s_- = 0$ and $s_+ = r_0$. Then, since $r_1 > r_0$, it can be verified that $Q_a(u)$ satisfies (2.2) on the interval $[s_-, s_+]$. In the comparisons below, we chose $r_0 = 1.3$. For this value of r_0 , we numerically obtain that

$$a_- = 2.2500, \quad \nu_- = 2.5886, \quad \beta = 1.8058, \quad \theta_- = .5599, \quad (3.3)$$

$$\theta_+ = 1.0634, \quad \mu = 2.6834.$$

These heteroclinic orbit constants, which are needed in (2.19)–(2.21), were obtained from a careful numerical computation of the heteroclinic connection $u_s(z)$ defined in (2.6).

For (2.1), the transient process associated with the initial formation of a pattern of well-defined internal layers from initial data is very intricate. In contrast to the Allen-Cahn equation, it is not clear which initial data will lead to a two-layer metastable pattern. To overcome this difficulty, a certain spatially dependent forcing term was added to the right side of (2.1) for a very short duration. The inclusion of such a term gave us the flexibility of routinely generating two-layer patterns with reasonably precise control on the locations of the internal layers at the onset of the metastable evolution. At some fixed $O(1)$ time, these initial internal layer locations computed from the numerical method were used as initial conditions for the asymptotic result (2.19a). The asymptotic and numerical results for $d_0 = d_0(t)$ were then compared at later times.

In Figure 2, we plot the asymptotic and numerical results for $\log_{10}(t)$ versus d_0 for some trajectories corresponding to two-layer metastable patterns for the Cahn-Hilliard equation ($\alpha = 0$). The values of ϵ used are indicated in this figure. On this logarithmic scale, the asymptotic and numerical results are indistinguishable. The three trajectories on the left side of Figure 2 correspond to $Q = Q_a$. For these trajectories, the layer centered at $x = x_0$ eventually collapses against the wall at $x = -1$. For the trajectory in Figure 2 with $\epsilon = .08$ and $Q = Q_a$, we plot the

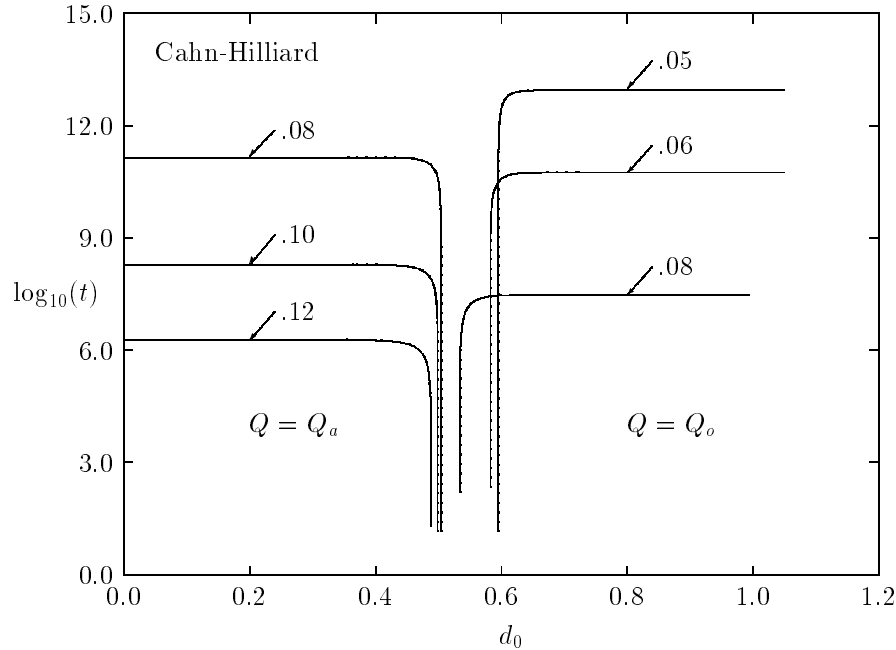


FIGURE 2. Asymptotic and numerical results for $\log_{10}(t)$ versus d_0 are shown for the Cahn-Hilliard equation ($\alpha = 0$). The labels indicate the values of ϵ used. The three trajectories on the left side correspond to the asymmetric form $Q = Q_a$ given in (3.2) with $r_0 = 1.3$, and the three trajectories on the right side are for $Q = Q_o = 2(u - u^3)$. In this plot, the asymptotic and numerical results are indistinguishable.

numerical solution in Figure 3 at several values of t . The collapse process, which occurs when $t \approx 1.391 \times 10^{11}$, is evident from this figure. A formal scaling suggests that the time scale for the completion of this collapse event is $O(1)$. The three curves on the right side of Figure 2 correspond to $Q = Q_o$. For these trajectories, the layer centered at $x = x_1$ eventually collapses against the wall at $x = 1$. The last point on each of these trajectories corresponds to the initiation of the collapse event, defined as the time for which $d_2 = 0$, where $d_2 = 1 - x_1$. Since the asymptotic result (2.19a) is not valid when a collapse event occurs, we do not compare the asymptotic and numerical results for d_0 at times during or after the collapse event. However, further numerical results (not shown) indicate that d_0 changes by an amount of $O(\epsilon)$ during the collapse event. After the layer collapse is complete, d_0 remains fixed at an equilibrium value consistent with a one-layer pattern with the same mass.

In Table 1a, we give a pointwise comparison of the asymptotic and numerical results for $d_0 = d_0(t)$ corresponding to the trajectory shown in Figure 2 with $Q = Q_o$ and $\epsilon = .05$. For the trajectory in Figure 2 with $Q = Q_a$ and $\epsilon = .08$, a similar comparison is shown in Table 1b. In these tables, the third and fourth columns compare the numerical and asymptotic elapsed times necessary for the distance d_0 to be given by the values in the first column. These elapsed times are found to agree to several

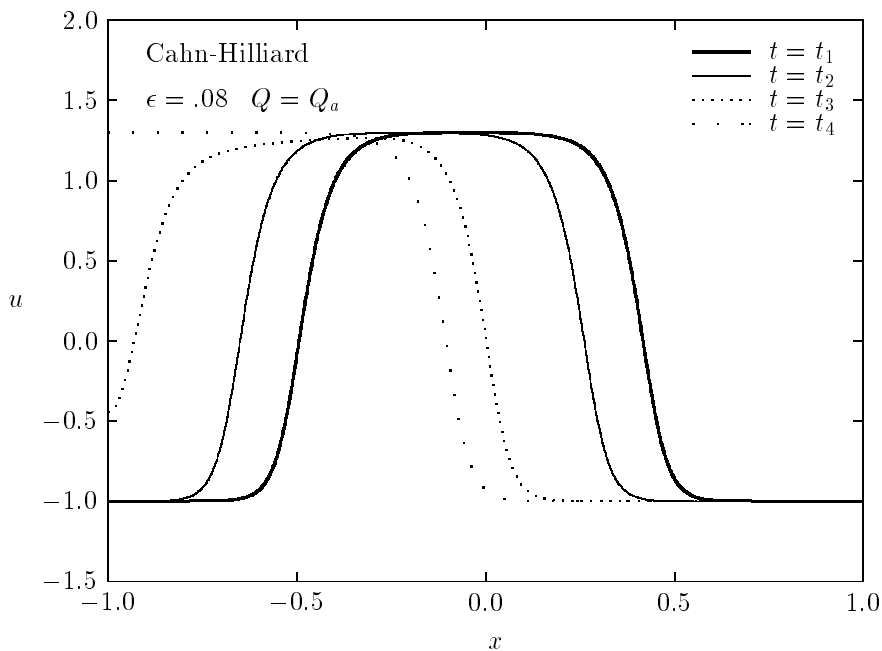


FIGURE 3. Plots of the numerical solution to the Cahn-Hilliard equation at different times corresponding to the parameter values given in the caption of Table 1b. The times are $t_1 = 22.42$, $t_2 = 1.3912861374 \times 10^{11}$, $t_3 = 1.3913503805 \times 10^{11}$, and $t_4 = 1.3921798980 \times 10^{11}$. The internal layer centered at $x = x_0$ collapses when $t \approx t_3$. The duration of this collapse process is presumably $O(1)$.

d_0 (num.)	d_0 (asy.)	t (num.)	t (asy.)
0.594993643	0.594993644	0.4692459394 ⁹	0.4686297431 ⁹
0.595235288	0.595235293	0.1698851766 ¹²	0.1698817367 ¹²
0.62484401	0.62484390	0.8036521829 ¹³	0.8036528889 ¹³
0.64538629	0.64538463	0.8691830759 ¹³	0.8691851609 ¹³
0.6653888	0.6653782	0.8817175084 ¹³	0.8817202122 ¹³
0.675509	0.675484	0.8834767270 ¹³	0.8834795897 ¹³
0.687090	0.687024	0.8843288486 ¹³	0.8843318111 ¹³
0.705747	0.705447	0.8847617813 ¹³	0.8847648277 ¹³
0.72468	0.72336	0.8848597065 ¹³	0.8848627831 ¹³
0.75191	0.74332	0.8848841878 ¹³	0.8848872775 ¹³
0.77372	0.75001	0.8848867648 ¹³	0.8848898570 ¹³
0.81901	0.75198	0.8848872950 ¹³	0.8848903883 ¹³

TABLE 1A. (Cahn-Hilliard) Results for $d_0 = d_0(t)$ for $Q(u) = 2(u - u^3)$ and $\epsilon = .05$. The initial values $x_0^0 = -.40500702$ and $x_1^0 = .54527721$ at $t = 14.42$ were used to calibrate the asymptotic results.

d_0 (num.)	d_0 (asy.)	t (num.)	t (asy.)
0.503717325	0.503717322	0.1327227942 ¹⁰	0.1327200053 ¹⁰
0.497710755	0.497711032	0.4580219562 ¹¹	0.4580387414 ¹¹
0.48854744	0.48854860	0.8758363748 ¹¹	0.8758748210 ¹¹
0.4774683	0.4774721	0.1139719166 ¹²	0.1139779931 ¹²
0.4551146	0.4551366	0.1332133700 ¹²	0.1332218341 ¹²
0.444789	0.444835	0.1360995881 ¹²	0.1361085986 ¹²
0.430191	0.430314	0.1379550139 ¹²	0.1379644445 ¹²
0.415586	0.415908	0.1386765684 ¹²	0.1386862400 ¹²
0.38392	0.38631	0.1390760004 ¹²	0.1390858988 ¹²
0.36904	0.37468	0.1391125076 ¹²	0.1391224369 ¹²
0.31080	0.35720	0.1391345193 ¹²	0.1391444878 ¹²
0.18619	0.35642	0.1391350379 ¹²	0.1391450083 ¹²

TABLE 1B. (Cahn-Hilliard) Results for $d_0 = d_0(t)$ for $\epsilon = .08$ and $Q(u)$ given by (3.2) with $r_0 = 1.3$. The initial values $x_0^0 = -.49613511$ and $x_1^0 = .41551949$ at $t = 14.42$ were used to calibrate the asymptotic results.

significant digits. The first and second columns in these tables compare the numerical and asymptotic results for d_0 at the times given in the third column. These results for d_0 agree well up until the collapse time is approached. However, for times near the collapse time (the last few rows of Tables 1a and 1b), very small numerical errors in computing the elapsed time get reflected in significantly larger errors in determining d_0 . This sensitivity to small numerical errors results from the fact that the solution changes on a much shorter time scale at the onset of a collapse event. However, we emphasize that if our numerical method made a significantly larger, but still rather modest, error in computing the elapsed time of say 1–2%, the asymptotic and numerical results for d_0 would agree rather poorly over a wide range.

In Figure 4, we plot asymptotic and numerical results for $\log_{10}(t)$ versus d_0 corresponding to two-layer patterns for the constrained Allen-Cahn equation (2.3) ($\alpha = 1$ and $\kappa = 1$ in (2.20)). The asymptotic and numerical results for $d_0(t)$ are again indistinguishable in this figure. For two of the trajectories shown in Figure 4, we give a similar pointwise comparison of the asymptotic and numerical results for $d_0(t)$ in Tables 2a and 2b as was done in Tables 1a and 1b. As for the case of the Cahn-Hilliard equation, the results in Tables 2a and 2b show that the values for the elapsed times are in very close agreement whereas the asymptotic and numerical results for d_0 at a given time agree well only up until a collapse event is initiated.

Finally, in Figure 5 we plot some trajectories $\log_{10}(t)$ versus d_0 corresponding to two-layer patterns for the viscous Cahn-Hilliard equation with $\alpha = 0.5$ and $\kappa = 1$. For two of these trajectories, the close agreement between the asymptotic and numerical results for $d_0(t)$ is shown in Tables 3a and 3b.

These comparisons show that the asymptotic result (2.19a) gives a highly accurate determination of the exponentially slow motion associated with two-layer metastable patterns of (2.1) before any collapse event occurs. Moreover, the numerical method we use is able to track accurately the motion of the internal layers over very long time intervals.

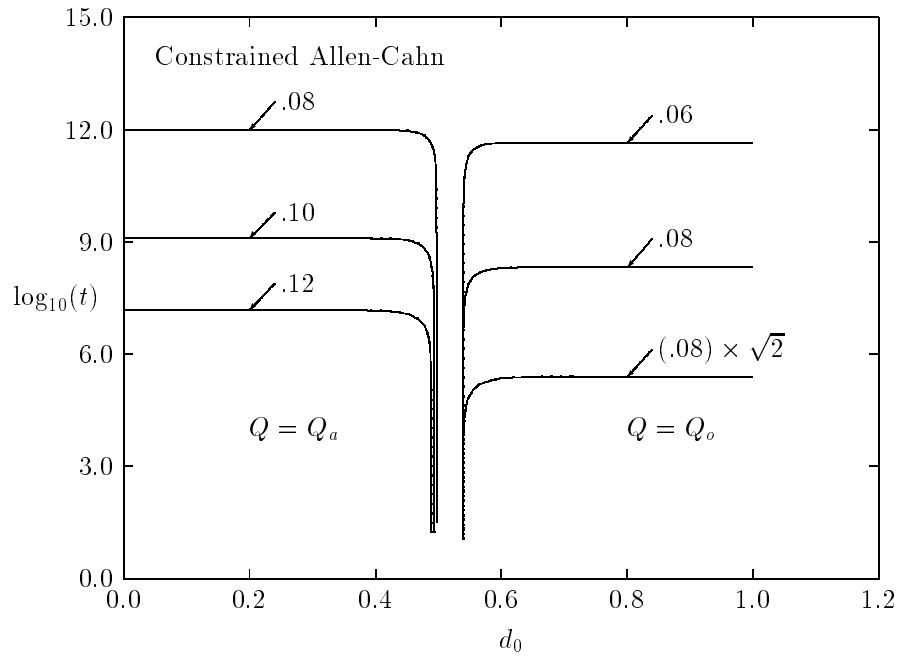


FIGURE 4. Asymptotic and numerical results for $\log_{10}(t)$ versus d_0 are shown for the constrained Allen-Cahn equation ($\alpha = 1$ and $\kappa = 1$). The labels in this figure have the same meaning as in Figure 2.

d_0 (num.)	d_0 (asy.)	t (num.)	t (asy.)
0.539778909	0.539778916	0.1327227944 ¹⁰	0.1327015589 ¹⁰
0.541108949	0.541108950	0.3882783312 ¹¹	0.3882780231 ¹¹
0.57881456	0.57880227	0.4093632517 ¹²	0.4093899505 ¹²
0.59818243	0.59813185	0.4330027517 ¹²	0.4330330269 ¹²
0.6143377	0.6141808	0.4389126267 ¹²	0.4389447181 ¹²
0.629264	0.628835	0.4408367720 ¹²	0.4408695100 ¹²
0.638418	0.637631	0.4413521681 ¹²	0.4413851863 ¹²
0.648952	0.647397	0.4416614057 ¹²	0.4416945959 ¹²
0.668908	0.663698	0.4418847440 ¹²	0.4419181011 ¹²
0.69137	0.67560	0.4419470211 ¹²	0.4419804571 ¹²
0.71876	0.68079	0.4419620534 ¹²	0.4419955324 ¹²
0.77414	0.68200	0.4419648636 ¹²	0.4419983546 ¹²

TABLE 2A. (Constrained Allen-Cahn) Results for $d_0 = d_0(t)$ for $Q(u) = 2(u - u^3)$, $\kappa = 1$, and $\epsilon = .06$. The initial values $x_0^0 = -.46026604$ and $x_1^0 = .53973846$ at $t = 21.67$ were used to calibrate the asymptotic results.

d_0 (num.)	d_0 (asy.)	t (num.)	t (asy.)
0.497154336	0.497155391	0.5308911772 ¹⁰	0.5374898994 ¹⁰
0.493154215	0.493155776	0.2256800766 ¹²	0.2257554296 ¹²
0.48899481	0.48899736	0.4016019371 ¹²	0.4016960215 ¹²
0.48582681	0.48583008	0.5071550534 ¹²	0.5072533120 ¹²
0.4784563	0.4784628	0.6830769138 ¹²	0.6831968268 ¹²
0.463235	0.463256	0.8633968208 ¹²	0.8635372035 ¹²
0.440003	0.440104	0.9469597045 ¹²	0.9471157040 ¹²
0.428362	0.428579	0.9596040882 ¹²	0.9597634019 ¹²
0.413773	0.414333	0.9664760358 ¹²	0.9666376186 ¹²
0.40298	0.40409	0.9686750591 ¹²	0.9688376802 ¹²
0.36963	0.37738	0.9705992045 ¹²	0.9707631907 ¹²
0.28957	0.36319	0.9708488494 ¹²	0.9710132102 ¹²

TABLE 2B. (Constrained Allen-Cahn) Results for $d_0 = d_0(t)$ for $\epsilon = .08$, $\kappa = 1$, and $Q(u)$ given by (3.2) with $r_0 = 1.3$. The initial values $x_0^0 = -.50275997$ and $x_1^0 = .40184203$ at $t = 32.67$ were used to calibrate the asymptotic results.

d_0 (num.)	d_0 (asy.)	t (num.)	t (asy.)
0.576222994	0.576222890	0.9384918795 ⁹	0.9386374332 ⁹
0.580142447	0.580142104	0.5764344397 ¹⁰	0.5764714039 ¹⁰
0.59223190	0.59222732	0.1470527387 ¹¹	0.1470747925 ¹¹
0.60218042	0.60216735	0.1820389844 ¹¹	0.1820714098 ¹¹
0.6159711	0.6159317	0.2043913081 ¹¹	0.2044303499 ¹¹
0.625185	0.625106	0.2111941892 ¹¹	0.2112362673 ¹¹
0.633463	0.633321	0.2145956298 ¹¹	0.2146394345 ¹¹
0.644669	0.644359	0.2170252302 ¹¹	0.2170708768 ¹¹
0.669233	0.667646	0.2187866905 ¹¹	0.2188342190 ¹¹
0.69671	0.68870	0.2191435381 ¹¹	0.2191916658 ¹¹
0.72685	0.69927	0.2192023800 ¹¹	0.2192506900 ¹¹
0.77022	0.70171	0.2192109808 ¹¹	0.2192593209 ¹¹

TABLE 3A. (Viscous Cahn-Hilliard) Results for $d_0 = d_0(t)$ for $Q(u) = 2(u - u^3)$, $\kappa = 1$, $\epsilon = .06$, and $\alpha = 0.5$. The initial values $x_0^0 = -.42443328$ and $x_1^0 = .57558911$ at $t = 21.37$ were used to calibrate the asymptotic results.

4. An n -layer metastable pattern for the viscous Cahn-Hilliard equation

We now outline the derivation of a differential-algebraic system that describes the metastable dynamics of an n -layer pattern for (2.1). Before doing so, we first introduce some convenient notation.

For $j = 0, \dots, n$, we define ξ_j by $\xi_j = (-1)^j \xi_0$, where $\xi_0 = \pm 1$ specifies the orientation of the internal layer closest to $x = -1$. For $j = 0, \dots, n$, the triplet

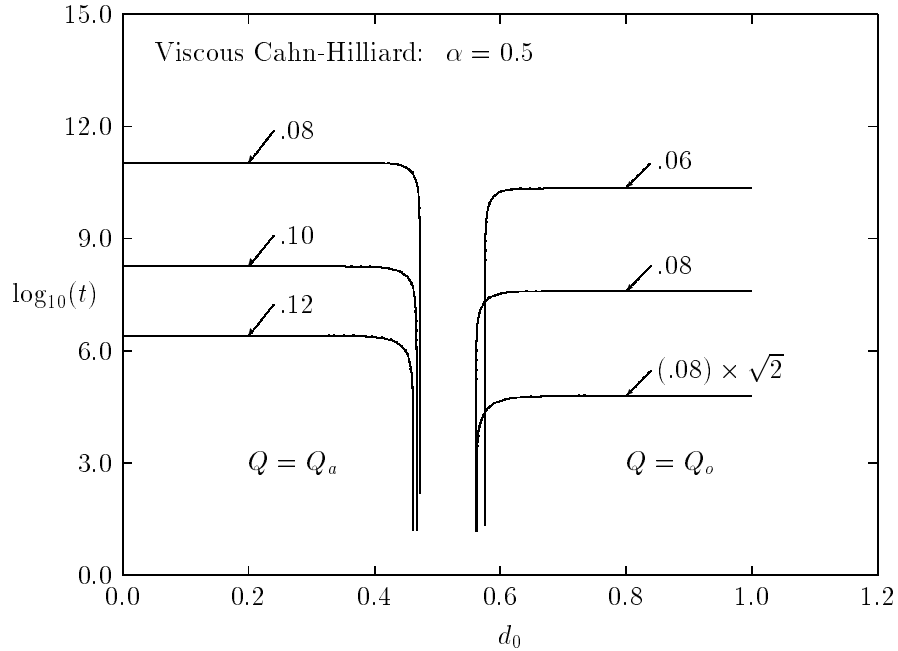


FIGURE 5. Asymptotic and numerical results for $\log_{10}(t)$ versus d_0 are shown for the viscous Cahn-Hilliard equation with $\alpha = 0.5$ and $\kappa = 1$. The labels in this figure have the same meaning as in Figure 2.

(a_j, ν_j, s_j) then is defined by

$$(a_j, \nu_j, s_j) = \begin{cases} (a_+, \nu_+, s_+) & \text{when } \xi_j = -1, \\ (a_-, \nu_-, s_-) & \text{when } \xi_j = +1. \end{cases} \quad (4.1)$$

Here a_{\pm} , ν_{\pm} , and s_{\pm} are given in (2.6b). An n -layer metastable pattern for (2.1) then is represented by the approximate form $u(x, t) \sim u^*(x)$, where

$$u^*(x) = u^*(x; x_0, \dots, x_{n-1}) \equiv u_s[\epsilon^{-1}\xi_0(x - x_0)] + \sum_{j=1}^{n-1} (u_s[\epsilon^{-1}\xi_j(x - x_j)] - s_j). \quad (4.2)$$

In (4.2), $x_j = x_j(t)$ for $j = 0, \dots, n-1$ and $x_{j-1}(t) < x_j(t)$. The inter-layer distances $d_j = d_j(t)$ are given by $d_j = x_j - x_{j-1}$ for $j = 0, \dots, n$, where we have introduced the fictitious layers x_{-1} and x_n by $x_{-1} = -1$ and $x_n = 1$. The layers are assumed to be well-separated in the sense that $d_j(t) = O(1)$ as $\epsilon \rightarrow 0$ for $j = 0, \dots, n$.

To derive equations of motion for $x_j(t)$, we use the projection method. The quasi-steady linearization of (2.4) is obtained by substituting $u(x, t) = u^*(x; x_0, \dots, x_{n-1}) +$

d_0 (num.)	d_0 (asy.)	t (num.)	t (asy.)
0.472285458	0.472285460	0.1466393880 ⁸	0.1467956085 ⁸
0.471197143	0.471197127	0.7185895526 ¹⁰	0.7185796612 ¹⁰
0.46663994	0.46663989	0.3228601659 ¹¹	0.3228579137 ¹¹
0.45877105	0.45877104	0.6148503132 ¹¹	0.6148499606 ¹¹
0.4435361	0.4435373	0.8905096190 ¹¹	0.8905224871 ¹¹
0.430504	0.430510	0.9839681073 ¹¹	0.9839946557 ¹¹
0.412817	0.412846	0.1032071741 ¹²	0.1032113656 ¹²
0.387096	0.387279	0.1050282402 ¹²	0.1050333008 ¹²
0.363111	0.364001	0.1053632477 ¹²	0.1053685853 ¹²
0.34605	0.34863	0.1054233772 ¹²	0.1054288057 ¹²
0.31707	0.32924	0.1054486102 ¹²	0.1054540964 ¹²
0.25333	0.32012	0.1054530981 ¹²	0.1054586002 ¹²

TABLE 3B. (Viscous Cahn-Hilliard) Results for $d_0 = d_0(t)$ for $\epsilon = .08$, $\alpha = 0.5$, $\kappa = 1$, and $Q(u)$ given by (3.2) with $r_0 = 1.3$. The initial values $x_0^0 = -.52771239$ and $x_1^0 = .37690138$ at $t = 161.43$ were used to calibrate the asymptotic results.

$w(x, t)$ into (2.4), under the assumption that $w \ll u^*$, $w_t \ll u_t^*$, and $\sigma \ll 1$. Then, in place of (2.8), we find

$$\epsilon^2 w_{xx} + Q'(u^*)w = \sigma + E(x) + \alpha \kappa u_t^*, \quad (4.3a)$$

$$w_x(-1, t) \sim -\epsilon^{-1} \xi_0 a_0 \nu_0 e^{-\epsilon^{-1} \nu_0 d_0}, \quad (4.3b)$$

$$w_x(1, t) \sim -\epsilon^{-1} \xi_{n-1} a_n \nu_n e^{-\epsilon^{-1} \nu_n d_n},$$

$$\sigma_{xx} = (1 - \alpha) \epsilon^{-1} \sum_{j=0}^{n-1} \xi_j \dot{x}_j u'_s[\epsilon^{-1} \xi_j (x - x_j)], \quad \sigma_x(\pm 1, t) = 0. \quad (4.3c)$$

Here $E(x) = E(x; x_0, \dots, x_{n-1})$ is given by

$$E(x; x_0, \dots, x_{n-1}) = \sum_{j=0}^{n-1} Q(u_s[\epsilon^{-1} \xi_j (x - x_j)]) - Q(u^*). \quad (4.4)$$

Next, we integrate (4.3c) to obtain

$$\begin{aligned} \sigma(x, t) &= (1 - \alpha) \sum_{j=0}^{n-1} \dot{x}_j M_j(x; x_j) + \sigma_c(t), \\ M_j(x; x_j) &= \int_{-1}^x (u_s[\epsilon^{-1} \xi_j (\eta - x_j)] - s_j) d\eta. \end{aligned} \quad (4.5)$$

When the approximation $m = \int_{-1}^1 u^*(x; x_0, \dots, x_{n-1}) dx$ to the mass constraint holds, the boundary conditions $\sigma_x(\pm 1, t) = 0$ are satisfied to within exponentially small terms that are negligible.

The eigenvalue problem (2.13), with u^* given in (4.2), has exactly n exponentially small eigenvalues λ_j for $j = 0, \dots, n-1$ (cf. [5]). For $\epsilon \rightarrow 0$, the corresponding normalized eigenfunctions are $\phi_j(x) \sim R_j u'_s[\epsilon^{-1} \xi_j (x - x_j)]$ for $j = 0, \dots, n-1$, where

R_j is a normalization constant. Substituting (4.5) into (4.3a) and expanding w as in (2.14a), we derive (2.14b). By imposing the limiting solvability conditions that $A_j = 0$ for $j = 0, \dots, n-1$, we obtain the coupled system for $\sigma_c(t)$ and $x_j(t)$, $j = 0, \dots, n-1$,

$$(1 - \alpha) \sum_{k=0}^{n-1} \dot{x}_k (M_k, \phi_j) + (\sigma_c, \phi_j) + \alpha \kappa (u_t^*, \phi_j) \sim B_j - (E, \phi_j), \quad (4.6)$$

$$j = 0, \dots, n-1.$$

Here B_j is defined in (2.14b). A further equation, which is given below in (4.7b), is obtained by evaluating the approximate mass constraint $m = \int_{-1}^1 u^*(x; x_0, \dots, x_{n-1}) dx$ for $\epsilon \rightarrow 0$.

Next, the asymptotic form $\phi_j(x) \sim R_j u'_s[\epsilon^{-1} \xi_j(x - x_j)]$ is used to evaluate the various terms in (4.6) for $\epsilon \rightarrow 0$. The terms B_j and (E, ϕ_j) were evaluated in [21], and it is easy to show that $(u_t^*, \phi_j) \sim -\xi_j \dot{x}_j \beta R_j$ and $(\sigma_c, \phi_j) \sim \epsilon \sigma_c(s_+ - s_-) R_j$. The substitution of these asymptotic formulas into (4.6) leads to the following result.

Proposition 2. *For $\epsilon \rightarrow 0$, an n -layer metastable pattern for (2.1) with widely spaced internal layers is represented by (4.2), where $x_j(t)$ for $j = 0, \dots, n-1$ and $\sigma_c(t)$ satisfy the differential-algebraic system*

$$\alpha \kappa \beta \dot{x}_j + \epsilon (1 - \alpha) \sum_{k=0}^{n-1} \dot{x}_k b_{jk} \sim \epsilon \sigma_c \xi_j(s_+ - s_-) + \epsilon H_j, \quad j = 0, \dots, n-1, \quad (4.7a)$$

$$\sum_{k=0}^n s_k (x_k - x_{k-1}) \sim m - \epsilon n (\theta_- - \theta_+). \quad (4.7b)$$

The exponentially weak forces H_j for $j = 0, \dots, n-1$ and the coupling coefficients b_{jk} for $j, k = 0, \dots, n-1$ are defined by

$$H_j = 2(a_{j+1}^2 \nu_{j+1}^2 e^{-(1+\delta_{j,n-1})\epsilon^{-1}\nu_{j+1}d_{j+1}} - a_j^2 \nu_j^2 e^{-(1+\delta_{j,0})\epsilon^{-1}\nu_j d_j}), \quad (4.8a)$$

$$b_{jk} = \int_{-1}^1 (u_s[\epsilon^{-1} \xi_k(x - x_k)] - s_k) (u_s[\epsilon^{-1} \xi_j(x - x_j)] - s_{j+1}) dx. \quad (4.8b)$$

In (4.7) and (4.8), (a_j, ν_j, s_j) , θ_{\pm} , and β are given in (4.1), (2.16b), and (2.18b), respectively. Also, in (4.8a), $\delta_{j,k}$ is the Kronecker symbol.

For the constrained Allen-Cahn equation where $\alpha = 1$ and $\kappa = 1$, (4.7) reduces to the result derived in [21]. Furthermore, if we set $\alpha = 1$, $\kappa = 1$, and $\sigma_c = 0$ in (4.7a) and disregard the mass constraint (4.7b), then (4.7a) reduces to the well-known dynamics $\dot{x}_j \sim \epsilon \beta^{-1} H_j$ associated with the unconstrained Allen-Cahn equation.

The coefficients b_{jk} in (4.7a) can be evaluated asymptotically for $\epsilon \rightarrow 0$ in a way similar to that shown in Appendix A for the two-layer case. A straightforward but lengthy calculation shows that

$$b_{jk} \sim -(-1)^{j+k} (x_j - x_k)(s_+ - s_-)^2$$

$$- \epsilon [1 - (-1)^{j+k}] \xi_j(s_+ - s_-)(\theta_- - \theta_+), \quad \text{for } j > k, \quad (4.9)$$

$$b_{jj} \sim -\epsilon \mu, \quad b_{jk} = O(e^{-\epsilon^{-1}c}), \quad \text{for } j < k.$$

Here μ is given in (2.18b) and c is a positive constant that is proportional to the distance $x_k - x_j$. From these asymptotic estimates for b_{jk} , it follows that if we write the left side of (4.7a) in the matrix form $B\dot{\mathbf{x}}$, then the matrix B is lower triangular

to within exponentially small terms. Moreover, if $0 < \alpha \leq 1$, then the entries in the matrix B that are below the main diagonal are $O(\epsilon)$ smaller than the entries along the main diagonal.

Since, for $0 < \alpha \leq 1$, B is a diagonal matrix to within $O(\epsilon)$ terms, the system (4.7) can be asymptotically decoupled for this range of α to obtain

$$\alpha\kappa\beta\dot{x}_j \sim \epsilon\xi_j n^{-1}(s_+ - s_-)^{-1} \sum_{k=0}^{n-1} (s_k - s_{k+1})H_k + \epsilon H_j, \quad j = 0, \dots, n-1, \quad (4.10a)$$

$$\sigma_c \sim n^{-1}(s_+ - s_-)^{-2} \sum_{k=0}^{n-1} (s_k - s_{k+1})H_k. \quad (4.10b)$$

When $\alpha = 1$, the form (4.10) is an exact reformulation of (4.7). In (4.10a), let $n > 2$ and label the initial-layer separations $d_j(0)$ for $j = 0, \dots, n$ by $d_j^0 = d_j(0)$. Assume that for some J with $J \neq 0$ and $J \neq n$ that $\nu_J d_J^0 < \nu_j d_j^0$ for all $j = 0, \dots, n$ and $j \neq J$. Then, from (4.10a), it is easy to show that the distance $d_J(t)$ between x_J and x_{J-1} satisfies the approximate evolution equation

$$d_J' \sim -\frac{4\epsilon}{\alpha\kappa\beta} \left(1 - \frac{2}{n}\right) a_J^2 \nu_J^2 e^{-\epsilon^{-1}\nu_J d_J}, \quad d_J(0) = d_J^0 > 0. \quad (4.11)$$

Integrating (4.11), we obtain

$$d_J(t) \sim d_J^0 + \frac{\epsilon}{\nu_J} \log[1 - t/t_s], \quad t_s \equiv \frac{\alpha\kappa\beta[1 - 2/n]^{-1}}{4a_J^2 \nu_J^3} e^{\epsilon^{-1}\nu_J d_J^0}. \quad (4.12)$$

Thus, $d_j = O(\epsilon)$ when $t \approx t_s$. The collapse time for the corresponding unconstrained Allen-Cahn equation is obtained by letting $n \rightarrow \infty$ and setting $\alpha = 1$ and $\kappa = 1$ in (4.12). A more detailed study and comparison of the internal layer dynamics (4.7) associated with the various limiting forms of (2.1) is in progress.

5. Artificial boundary conditions and spurious metastable dynamics

Domain truncation with the imposition of a simple form of artificial boundary condition can significantly perturb the metastable internal layer dynamics associated with problems defined on infinite domains. To illustrate this effect, we consider the Allen-Cahn problem that results from truncating an infinite domain problem to the finite domain problem

$$u_t = \epsilon^2 u_{xx} + Q(u), \quad -L < x < L, \quad t > 0, \quad (5.1a)$$

$$\epsilon u_x(L, t) = -\nu[u(L, t) - 3s], \quad \epsilon u_x(-L, t) = \nu[u(-L, t) + s]. \quad (5.1b)$$

Here $L > 0$, $s > 0$, and $Q(u)$ is an odd periodic function satisfying $Q(-s) = 0$, $Q'(-s) < 0$, and $Q(u + 2s) = Q(u)$. The simple artificial boundary conditions (5.1b), where $\nu = [-Q'(-s)]^{1/2}$, were derived by linearizing (5.1a) about the constant states $u = -s$ and $u = 3s$ and then by finding the decay rates onto the constant states. The corresponding nontruncated problem is (5.1a) on the infinite line $-\infty < x < \infty$ with $u \rightarrow -s$ as $x \rightarrow -\infty$ and $u \rightarrow 3s$ as $x \rightarrow \infty$. For the form of u shown in Figure 6, our goal is to compare the metastable internal layer dynamics for the infinite domain problem with that of the truncated problem (5.1) (see [24] for some related work).

The metastable pattern shown in Figure 6 is represented by $u(x, t) \sim u^*(x)$, where

$$u^*(x) = u^*(x; x_0, x_1) \equiv u_s[\epsilon^{-1}(x - x_0)] + u_s[\epsilon^{-1}(x - x_1)] + s. \quad (5.2)$$

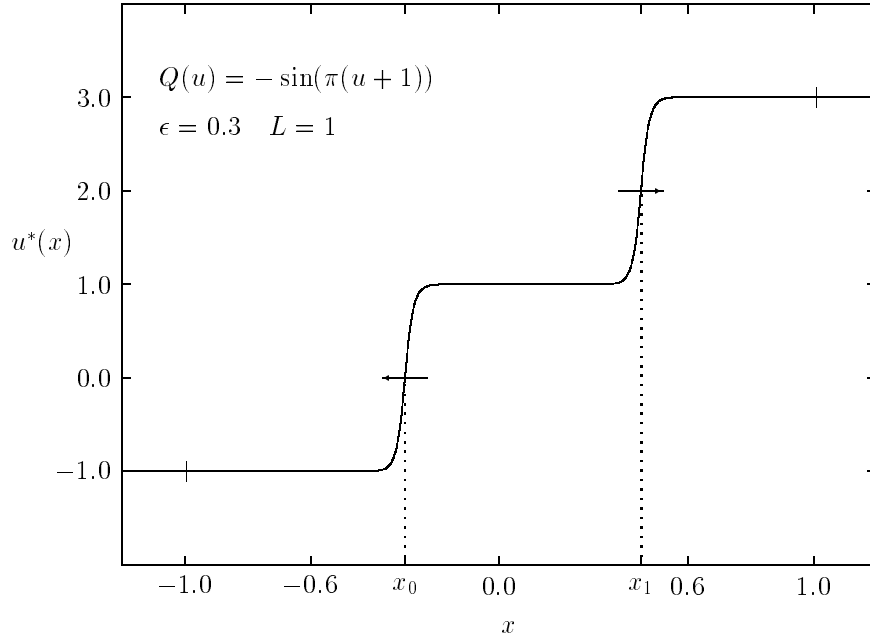


FIGURE 6. Plot of $u^*(x)$ given by (5.2) with $u_s(z) = 4\pi^{-1} \tan^{-1}(e^{\sqrt{\pi}z}) - 1$ and $s = 1$, that approximates a two-layer metastable pattern for (5.1). The artificial boundary conditions (5.1b) are applied at $L = 1$. On the infinite line, the motion of the internal layers for all time is in the direction of the arrows.

Here $x_j = x_j(t)$ and $x_0 < x_1$. In (5.2), the heteroclinic orbit $u_s(z)$ satisfies (2.6a) and the anti-symmetry condition $u_s(z) = -u_s(-z)$. By retaining an extra term in the far field form of $u_s(z)$, we derive from (2.6a) that

$$u_s(z) \sim s - ae^{-\nu z} + be^{-k\nu z} + \dots \quad z \rightarrow \infty \quad (5.3)$$

In (5.3), a , b , and k are defined by

$$\begin{aligned} \log\left(\frac{a}{s}\right) &= \int_0^s \left(\frac{\nu}{[2V(\eta)]^{1/2}} + \frac{1}{\eta - s} \right) d\eta, \\ V(u) &= - \int_s^u Q(\eta) d\eta, \\ k = 2, \quad b &= -\frac{a^2 Q''(s)}{6\nu^2}, \quad \text{for } Q''(s) \neq 0; \\ k = 3, \quad b &= \frac{a^3 Q'''(s)}{48\nu^2}, \quad \text{for } Q''(s) = 0. \end{aligned} \quad (5.4)$$

To derive equations of motion for $x_0(t)$ and $x_1(t)$, we use the projection method. Let $u = u^* + w$, where $w \ll u^*$ and $w_t \ll u_t^*$. Then, from (5.1) and (5.3), the

quasi-steady linearized problem for w is

$$\epsilon^2 w_{xx} + Q'(u^*)w = E(x) + u_t^*, \quad -L < x < L, \quad (5.5a)$$

$$\epsilon w_x(-L, t) - \nu w(-L, t) = (k-1)b\nu e^{-\epsilon^{-1}k\nu(L+x_0)}, \quad (5.5b)$$

$$\epsilon w_x(L, t) + \nu w(L, t) = (k-1)b\nu e^{-\epsilon^{-1}k\nu(L-x_1)}. \quad (5.5c)$$

In (5.5a), E is defined upon substituting $\xi_0 = 1$, $\xi_1 = 1$, $n = 2$, and (5.2) into (4.4). On the interval $|x| < L$, the eigenvalue problem associated with (5.5) is (2.13a) with boundary conditions $\epsilon\phi'(\pm L) \pm \nu\phi(\pm L) = 0$. For $\epsilon \rightarrow 0$, the (nonnormalized) eigenfunctions corresponding to the two exponentially small eigenvalues are $\phi_j(x) \sim u'_s[\epsilon^{-1}(x - x_j)]$ for $j = 0, 1$. In the limit $\epsilon \rightarrow 0$, we enforce the solvability conditions that the projections of w against these eigenfunctions are zero. From these conditions, we obtain the coupled system of differential equations for $x_0(t)$ and $x_1(t)$ given by

$$\epsilon^{-1}\beta\dot{x}_0 \sim -2a^2\nu^2 e^{-\epsilon^{-1}\nu d_1} + (k-1)ba\nu^2 e^{-\epsilon^{-1}(k+1)\nu d_0}, \quad (5.6a)$$

$$\epsilon^{-1}\beta\dot{x}_1 \sim 2a^2\nu^2 e^{-\epsilon^{-1}\nu d_1} - (k-1)ba\nu^2 e^{-\epsilon^{-1}(k+1)\nu d_2}. \quad (5.6b)$$

In (5.6), β is given in (2.18b), $d_1 = x_1 - x_0$, $d_0 = x_0 + L$, and $d_2 = L - x_1$.

We now interpret the dynamics (5.6). On the infinite line, the distance between x_1 and x_0 satisfies $\dot{d}_1 \sim 4\epsilon\beta^{-1}a^2\nu^2 e^{-\epsilon^{-1}\nu d_1}$. Thus, the inter-layer force is repulsive for all d_1 and $d_1 \rightarrow \infty$ as $t \rightarrow \infty$. Now for the truncated problem, the last terms on the right sides of (5.6a,b) can be neglected in the limit $\epsilon \rightarrow 0$ only when $d_1 < (k+1)\min(d_0, d_2)$. Thus, it is only for this range of d_1 that the metastable dynamics of the truncated problem correctly approximates that of the infinite domain problem. As d_1 increases, the last terms on the right sides of (5.6a,b) become more significant and spurious effects from the artificial boundary conditions are introduced. When $b > 0$, these conditions have the deleterious effect of introducing a *spurious stable steady-state solution* not present in the infinite domain problem. The equilibrium layer spacings d_{0e} , d_{1e} , and d_{2e} for this steady solution are

$$\begin{aligned} d_{0e} = d_{2e} &\sim \frac{2L}{k+3} - \frac{\epsilon}{\nu(k+3)} \log \gamma, \\ d_{1e} &\sim \frac{2L(k+1)}{k+3} + \frac{2\epsilon}{\nu(k+3)} \log \gamma. \end{aligned} \quad (5.7)$$

Here $\gamma \equiv 2a/[(k-1)b]$. To illustrate the theory, let $Q(u) = -\sin[\pi(u+1)]$. For this example, $k = 3$, $a = 4\pi^{-1}$, $\nu = \sqrt{\pi}$, and $b = 4/(3\pi)$. From (5.7), it then follows that $d_{1e} \sim 4L/3 + \epsilon \log(3)/(3\sqrt{\pi})$ and $d_{0e} = d_{2e} = L/3 + O(\epsilon)$. Thus, the interesting qualitative feature in this problem is that the artificial boundary conditions can induce spurious metastable dynamics even when the internal layers are located at an $O(1)$ distance away from where the artificial boundary conditions are imposed.

There are many other problems defined on the infinite line where various types of localized structures interact with each other by way of exponentially weak inter-layer forces. Examples of such problems include the interaction of solitary waves of nearly equal amplitude for the KdV equation and related equations, and the interaction of kinks for nonlinear wave equations. To numerically solve these more general problems using finite difference methods, the infinite domain must be truncated to a finite domain and artificial boundary conditions must be imposed. The simple example analyzed above suggests that considerable care must be taken in performing

these computations to ensure that any spurious dynamics introduced by the artificial boundary conditions does not obscure the delicate interaction between the localized structures.

Appendix A. Evaluation of the inner products for a two-layer pattern

For $\epsilon \rightarrow 0$, we now outline the evaluation of the inner products (M_j, ϕ_k) for $j = 0, 1$ and $k = 0, 1$, given in (2.18a). Here $\phi_k \sim R_k u'_s [(-1)^k \epsilon^{-1} (x - x_k)]$ and M_j is defined in (2.12).

To evaluate (M_0, ϕ_0) , we first integrate by parts to obtain

$$\begin{aligned} (M_0, \phi_0) &= -\epsilon R_0 \int_{-1}^1 u_s[\epsilon^{-1}(x - x_0)] (u_s[\epsilon^{-1}(x - x_0)] - s_-) dx \\ &\quad + \epsilon R_0 u_s[\epsilon^{-1}(1 - x_0)] \int_{-1}^1 (u_s[\epsilon^{-1}(x - x_0)] - s_-) dx. \end{aligned} \quad (\text{A.1})$$

Combining the integrals in (A.1) and using $u_s[\epsilon^{-1}(1 - x_0)] \sim s_+$ for $\epsilon \rightarrow 0$, we derive

$$(M_0, \phi_0) \sim \epsilon R_0 \int_{-1}^1 (s_+ - u_s[\epsilon^{-1}(x - x_0)]) (u_s[\epsilon^{-1}(x - x_0)] - s_-) dx. \quad (\text{A.2})$$

The dominant contribution to the integral in (A.2) arises from the region near $x = x_0$. In this way, we find that $(M_0, \phi_0) \sim \epsilon^2 \mu R_0$, where μ is defined in (2.18b). A similar calculation shows that $(M_1, \phi_1) \sim -\epsilon^2 \mu R_1$.

To evaluate (M_1, ϕ_0) , we integrate by parts and then combine the resulting integrals to derive

$$(M_0, \phi_1) \sim \epsilon R_1 \int_{-1}^1 (u_s[\epsilon^{-1}(x_1 - x)] - s_-) (u_s[\epsilon^{-1}(x - x_0)] - s_-) dx. \quad (\text{A.3})$$

The right side of (A.3) can be written exactly in the more convenient form

$$\begin{aligned} (M_0, \phi_1) &\sim 2\epsilon R_1 (s_+ - s_-)^2 + \epsilon R_1 (s_+ - s_-) \int_{-1}^1 (u_s[\epsilon^{-1}(x - x_0)] - s_+) dx \\ &\quad + \epsilon R_1 (s_+ - s_-) \int_{-1}^1 (u_s[\epsilon^{-1}(x_1 - x)] - s_+) dx \\ &\quad + \epsilon R_1 \int_{-1}^1 (u_s[\epsilon^{-1}(x - x_0)] - s_+) (u_s[\epsilon^{-1}(x_1 - x)] - s_+) dx. \end{aligned} \quad (\text{A.4})$$

Since the last integral on the right side of (A.4) is $O(e^{-\epsilon^{-1}c})$ for some $c > 0$, it can be neglected. Next, for $\epsilon \rightarrow 0$, we evaluate the remaining two integrals in (A.4) to get

$$\begin{aligned} \int_{-1}^1 (u_s[\epsilon^{-1}(x - x_0)] - s_+) dx &\sim -(x_0 + 1)(s_+ - s_-) + \epsilon(\theta_- - \theta_+), \\ \int_{-1}^1 (u_s[\epsilon^{-1}(x_1 - x)] - s_+) dx &\sim (1 - x_1)(s_- - s_+) + \epsilon(\theta_- - \theta_+). \end{aligned} \quad (\text{A.5})$$

Here θ_{\pm} are defined in (2.16b). The result for (M_0, ϕ_1) given in (2.18a) then is obtained by combining (A.4) and (A.5).

Finally, an integration by parts shows that (M_1, ϕ_0) is given by (A.3) where s_- and R_1 are replaced by s_+ and $-R_0$, respectively. Since the resulting integrand is

exponentially small for $-1 < x < 1$, it follows that $(M_1, \phi_0) = O(e^{-\epsilon^{-1}c})$ for some $c > 0$. Therefore, in deriving (2.19) from (2.15), we have set $(M_1, \phi_0) = 0$ in (2.15a).

References

1. N. Alikakos, P. W. Bates, and G. Fusco, *Slow motion for the Cahn-Hilliard equation in one space dimension*, J. Differential Equations **90** (1991), 81–135.
2. N. Alikakos and W. McKinney, *Remarks on the equilibrium theory for the Cahn-Hilliard equation in one space dimension*. In: Reaction-Diffusion Equations, (K. J. Brown and A. A. Lacey, eds.), Clarendon Press, Oxford, 1990, pp. 75–93.
3. L. Bronsard and D. Hilhorst, *On the slow dynamics for the Cahn-Hilliard equation in one space dimension*, Proc. Roy. Soc. London A **439** (1992), 669–682.
4. J. Cahn and J. Hilliard, *Free energy of a non-uniform system. I. Interfacial free energy*, J. Chem. Phys. **28** (1958), 258–267.
5. J. Carr and R. Pego, *Metastable patterns in solutions of $u_t = \epsilon^2 u_{xx} - f(u)$* , Comm. Pure Appl. Math. **42** (1989), 523–576.
6. J. Carr, M. Gurtin, and M. Slemrod, *Structural phase transitions on a finite interval*, Arch. Rational Mech. Anal., **86** (1984), 317–351.
7. G. Dahlquist and Å. Björck, *Numerical Methods*, Prentice-Hall Inc., Englewood Cliffs, NJ, 1974.
8. C. M. Elliot and D. A. French, *Numerical studies of the Cahn-Hilliard equation for phase separation*, IMA J. Appl. Math. **38** (1987), 97–128.
9. G. Fusco and J. Hale, *Slow motion manifold, dormant instability and singular perturbation*, J. Dynamics Diff. Equations **1**, (1989), 75–94.
10. C. W. Gear, *Numerical Initial Value Problems in Ordinary Differential Equations*, Prentice-Hall Inc., Englewood Cliffs, NJ, 1971.
11. C. Grant, *Slow motion in one-dimensional Cahn-Morral systems*, SIAM J. Math. Anal. **26** (1995), 21–34.
12. W. Henshaw, H. O. Kreiss, and L. G. Reyna, *A fourth-order accurate difference approximation for the incompressible Navier-Stokes equations*, Computers & Fluids **23** (1994), 575–593.
13. H. B. Keller, *Numerical solution of bifurcation and nonlinear eigenvalue problems*, In: Applications of Bifurcation Theory, (P. H. Rabinowitz, ed.), Academic Press, 1977, pp. 359–384.
14. G. Kreiss and H. Kreiss, *Convergence to steady state of solutions of Burgers equation*, Appl. Numerical Math. **2** (1986), 161–179.
15. M. Kuwamura, S. I. Ei, and M. Mimura, *Very slow dynamics for some reaction-diffusion systems of the activator-inhibitor type*, Japan J. Indust. Appl. Math. **9** (1992), 35–77.
16. J. Laforge and R. E. O'Malley, *Shock layer movement for Burgers equation*, SIAM J. Appl. Math. **55** (1995), 332–348.
17. J. J. Dongarra, C. B. Moler, J. R. Bunch, and G. W. Stewart, *LINPACK User's Guide*, SIAM, Philadelphia, PA, 1979.
18. J. Neu, unpublished notes (1984).
19. A. Novick-Cohen, *On the viscous Cahn-Hilliard equation*, In: Material Instabilities in Continuum Mechanics and Related Mathematical Problems (J. Ball, ed.), Oxford Science Publications, Clarendon Press, Oxford (1988), pp. 329–342.
20. A. Novick-Cohen and R. L. Pego, *Stable patterns in a viscous diffusion equation*, Trans. Amer. Math. Soc. **324** (1991), 331–351.
21. L. G. Reyna and M. J. Ward, *Resolving weak internal layer interactions for the Ginzburg-Landau equation*, European J. Appl. Math. **5** (1994), 495–523.
22. ———, *On the exponentially slow motion of a viscous shock*, Comm. Pure Appl. Math. **48** (1995), 79–120.
23. J. Rubinstein and P. Sternberg, *Nonlocal reaction-diffusion equations and nucleation*, IMA J. Appl. Math. **48** (1992), 249–264.
24. M. J. Ward and L. G. Reyna, *Internal layers, small eigenvalues and the sensitivity of metastable motion*, SIAM J. Appl. Math. **55** (1995), 425–445.
25. M. J. Ward, *Metastable patterns, layer collapses, and coarsening for a one-dimensional Ginzburg-Landau equation*, Studies Appl. Math. **91** (1994), 51–93.

MATHEMATICAL SCIENCES, I.B.M. THOMAS WATSON RESEARCH CENTER, YORKTOWN HEIGHTS, NEW YORK 10598

DEPARTMENT OF MATHEMATICS, UNIVERSITY OF BRITISH COLUMBIA, VANCOUVER, BRITISH COLUMBIA, V6T 1Z2